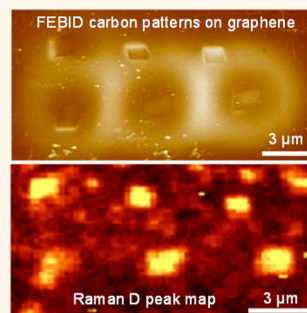# Controlling the Physicochemical State of Carbon on Graphene Using Focused Electron-Beam-Induced Deposition

Songkil Kim,[†] Dhaval D. Kulkarni,[‡] Richard Davis,[‡] Steve S. Kim,[⊥] Rajesh R. Naik,[⊥] Andrey A. Voevodin,[⊥] Michael Russell,[‡] Seung Soon Jang,[‡] Vladimir V. Tsukruk,[‡] and Andrei G. Fedorov[†,§,*]

[†]George W. Woodruff School of Mechanical Engineering, [‡]School of Materials Science and Engineering, and [§]Parker H. Petit Institute for Bioengineering and Bioscience, Georgia Institute of Technology, Atlanta, Georgia 30332, United States and [⊥]Materials and Manufacturing Directorate, Air Force Research Laboratory, Wright-Patterson AFB, Ohio 45433-7707, United States

ABSTRACT Focused electron-beam-induced deposition (FEBID) is a promising nanolithography technique using "direct-write" patterning by carbon line and dot deposits on graphene. Understanding interactions between deposited carbon molecules and graphene enables highly localized modification of graphene properties, which is foundational to the FEBID utility as a nanopatterning tool. In this study, we demonstrate a unique possibility to induce dramatically different adsorption states of FEBID-produced carbon deposits on graphene, through density functional theory calculations and complementary Raman experiments. Specifically, an amorphous carbon deposit formed by direct irradiation of high energy primary electrons exhibits unusually strong interactions with graphene *via* covalent bonding, whereas the FEBID carbon formed due to low-energy secondary electrons is only weakly interacting with graphene *via* physisorption. These observations not only are of fundamental importance to basic physical chemistry of FEBID carbon—graphene interactions but also enable the use of selective laser-assisted postdeposition ablation to effectively remove the parasitically deposited, physisorbed carbon films for improving FEBID patterning resolution.

FEBID carbon patterns on graphene
3 μm

Raman D peak map
3 μm

Focused electron-beam-induced deposition (FEBID) is an emerging chemical vapor deposition (CVD) method, enabling a resist-free "direct-write" additive nanomanufacturing using a variety of precursor materials with a high degree of control.[1,2] It is a versatile tool for localized, high-resolution 3D nanofabrication,[3,4] including electromechanical welding,[5−7] plasmonic nanostructures,[8] transistors,[9] magnetic sensors,[10] and nanocomposites.[11] FEBID process makes a deposit from nonvolatile residual species resulting from dissociation of adsorbed precursor molecules by low-energy secondary electrons, which are generated by high-energy, primary electrons of the focused beam upon interactions with a substrate.[1−4] In FEBID, the nature of interactions between the precursor molecules and a substrate has an important role in deposition.[2,12] Chemisorption of precursor molecules results in faster growth rates as well as higher purity of deposits, as compared to FEBID of physisorbed molecules.[12]

It can be achieved by heating a gaseous precursor to increase the kinetic and vibration energies of molecules yielding their higher reactivity upon interaction with surfaces[12] or by introducing the reactive sites[13] on a substrate.

On a graphene surface, which forms a two-dimensional hexagonal lattice structure of sp^2-bonded carbon atoms, electron irradiation can affect adsorption of precursor molecules or fragments since it can modify the local structure of graphene. A range of point-like defects can be controllably generated ranging from vacancies or Stone—Wales (SW) defects to sp^3-type defects, depending on the beam energy and doses.[14,15] These structural modifications of the highly inert graphene surface can reduce activation barriers for chemisorption of reactive radicals dissociated by electron beam at room temperature.[14,16] Unlike for a bulk substrate, chemisorption of reactive species on graphene has a significant impact in that it can tune the graphene's

electronic properties, including opening a band gap and enhancing spin−orbit coupling.[17−19]

Among a variety of possible "active" species suitable for functionalization, recent theoretical studies revealed that controlled chemisorption of carbon atoms or hydrocarbon radicals are particularly effective in modifying the electronic and magnetic properties of graphene.[20−24] Depending on adsorption state configuration and surface coverage, electromagnetic properties of graphene can be modulated, which illustrates the importance of controlled deposition of carbon atoms to enable applications of graphene for electronic and spintronic devices. Thus, nanoscale direct-write deposition by focused electron beam using hydrocarbon precursors provides an intriguing opportunity for controlled covalent functionalization of graphene by individual carbon atoms, resulting in localized, high-resolution patterning of a graphene substrate. In turn, this makes it possible to achieve an electron-beam-confined modification of electromagnetic properties of graphene-based materials since FEBID-produced carbon deposits can be easily transformed from insulating to graphitic structures with assistance of annealing techniques.[9,25−27]

Intrinsic resolution of FEBID carbon patterning on graphene is comparable to a diameter of the focused primary electron beam down to a few nanometers, which stresses its superiority in control of the patterning resolution.[28,29] However, such a high resolution is only feasible on suspended graphene. When graphene is supported by a bulk substrate, such as SiO_2/Si, as relevant to its application in electronic devices, unintentional hydrocarbon deposition and broadening of target patterns are inevitable due to a wide-range spatial distribution of secondary electrons.[1−4,28,29] This degrades the resolution of patterning, impeding a desirable level of spatial control of graphene functionalization. Thus, for successful application of FEBID technique to real device platforms, it is important to eliminate unintentional (parasitic) carbon deposits without introducing any structural defects or damage to graphene, which require the first-principle understanding of carbon−graphene interactions under different FEBID conditions.

In this study, we assess the nature of adsorption states of FEBID-produced carbon on graphene as a function of the deposit location and suggest a laser-assisted postdeposition process to remove parasitic carbon deposits. Using density functional theory (DFT) calculations, we first analyze an adsorption mechanism of methane-derived CH_n ($n = 1−3$) radicals on graphene in conjunction with the sp^3-type defect formation by high-energy electron beam irradiation. Guided by the calculation results, the interactions between FEBID-produced carbon deposits and graphene are subsequently investigated using Raman spectroscopy in conjunction with laser-induced ablation of thermally less stable, physisorbed carbon species. Collectively, these simulations and characterization experiments establish clear evidence for a controlled formation of different adsorption states of carbon deposits on graphene, depending on the type/energy of electrons contributing to the deposition process.

RESULTS AND DISCUSSION

DFT Simulations of the Effect of Electron-Beam-Induced sp^3-Type Graphene Defects on Molecular adsorption. Density functional theory calculations were performed to study adsorption of an isolated CH_3 radical onto a 4 × 4 supercell of graphene. A CH_3 radical is first in a sequence of intermediate species CH_n ($n = 1−3$) in the transformation of methane precursor (CH_4) to atomic carbon (C) by the FEBID process. As a reference state, CH_3 radical is placed on top of a carbon atom of graphene with the initial distance of ∼3 Å.[30] Adsorption structures were obtained for various sp^3-type defect heights (h) on graphene used as a configuration input parameter in DFT calculations to define the threshold height leading to chemisorption. Figure 1a, b shows a representative physisorption state of a CH_3 radical on a defect-free graphene and its chemisorption state on the defected graphene, respectively. The effect of defect heights on adsorption of CH_3 by graphene (Figure 1c) shows a threshold h value for chemisorption of ∼0.37 Å. Below this threshold height, CH_3 physisorbs on graphene with the binding distance (d_{Gr-CH_3}) over ∼3 Å and the binding energy (E_b) below ∼120 meV.[31] Otherwise, it chemisorbs on graphene with more than 13 times greater binding energy than that for the physisorption state. Here, the binding energy (E_b) is calculated as $E_b = E_{total}$(hybrid system) − E_{total}(graphene) − $E_{total}(CH_3)$.[32] In Figure 1d, the total energy for each structure is plotted to define the energy barrier for transition from physisorption to chemisorption *via* formation of a sp^3-type defect. The energy barrier is ∼0.9 eV, which corresponds to the formation energy of a sp^3-type defect with $h \sim 0.37$ Å. The formation energy (E_f) was calculated as the energy difference between defected and defect-free graphene, $E_f = E_{total}$(defected) − E_{total}(defect-free).[33]

Chemisorption of CH_3, demonstrated using the DFT calculations, can be facilitated by exposing graphene to the energetic primary beam electrons, leading to formation of structural defects on graphene as active sites for chemisorption. The maximum transferrable energy to one carbon atom by electron irradiation can be estimated using the Mckinley−Feshbach approximation.[14,34] For example, the primary electrons with energy of 25 keV, which is typical for the primary beam in FEBID, can transfer energy up to 4.8 eV to one carbon atom of graphene. It is much higher than the energy barrier for chemisorption of CH_3 onto graphene. It is worth noting that the transfer energy for the 25 keV electron is not large enough to generate the
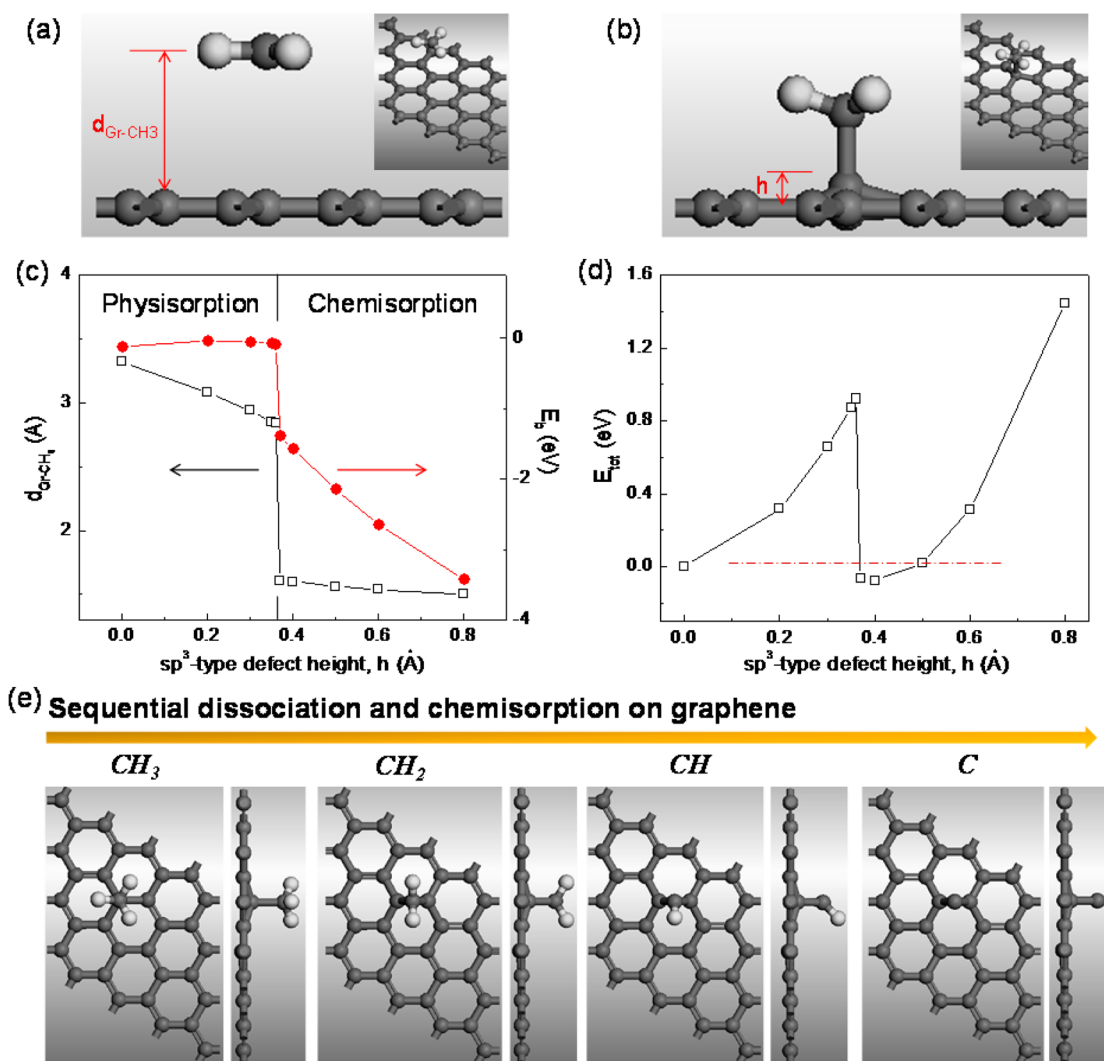
Figure 1. Adsorption states of a representative FEBID radical (CH_3) on graphene: (a) Physisorption on defect-free graphene and (b) chemisorption on graphene with a sp^3-type defect site generated by high-energy electron beam irradiation. Insets show the tilted views of the two adsorption structures. (c) Demonstration of transition from physisorption to chemisorption with dramatic change in binding distance and energy, induced by an increase of the graphene defect height, and (d) total energy changes showing an energy barrier for transition to the chemisorption state. (e) Chemisorbed structures of FEBID intermediate species resulting from dissociation of methane precursor on graphene by sequential cleaving of H atoms.

SW defects or a knock-on damage (vacancy formation) in graphene, which have energy barriers of 10 and 18−20 eV for their formation, respectively.[14] Thus, it can be expected that the primary electrons with energy of 25 keV generate sp^3-type defects on graphene, which along with simultaneous dissociation of CH_4 molecules to CH_3 radicals by secondary electrons result in chemisorption of CH_3 onto graphene. Once CH_3 is chemisorbed, sequential dissociation of H atoms by secondary electrons can lead to covalent bonding of each intermediate species CH_n ($n = 1,2$) to graphene, as shown in Figure 1e. The final product of an FEBID sequence with the CH_4 precursor is a carbon atom covalently bound on the bridge site (C−C bond) of graphene.[14,22−24]

Identification of FEBID Carbon Adsorption States Using Raman Spectroscopy. Using DFT calculations, we showed

two possible adsorption states of hydrocarbon radicals on graphene, depending on the formation of sp^3-type defects in graphene controlled by the primary electron energy. To experimentally demonstrate different adsorption states of FEBID carbon deposits on graphene, we performed a complementary Raman analysis of FEBID deposits on graphene. Raman spectroscopy is a standard tool for characterizing amorphous to crystalline carbon nanostructures.[26,35,36] In the Raman spectrum of carbon structures, signature characteristics are the G and D peaks appearing around 1500−1630 and 1340−1380 cm^{-1}, respectively.[26,27,35] The G peak is related to in-plane bond stretching of sp^2 carbon pairs.[35] The D peak is due to a breathing mode of sp^2 carbon atoms in six-fold rings, and it requires defects for its activation. Thus, a D peak in the spectrum is indicative of disorder in graphene/graphite, as well as the presence
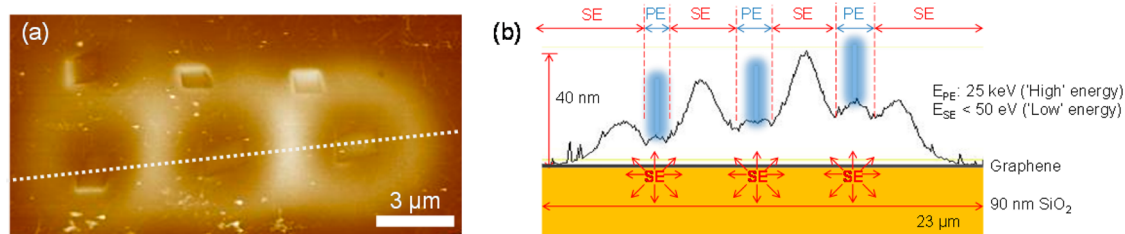
Figure 2. (a) AFM image of as-deposited FEBID carbon structures on CVD graphene, showing the patterned squares and halo film around them. (b) Schematic illustration showing FEBID carbon deposition process with the AFM cross-sectional profile of the bottom row FEBID carbon structure along the dotted line in (a). PE: primary electron. SE: secondary electron.

of graphitic domains in amorphous carbon.[26,35−37] As-deposited FEBID carbon is an amorphous mixture of sp^2 and sp^3 sites with hydrogen content up to 60%.[26,35] It can be thought as a hybrid composite structure of two separate carbon materials, with different interactions between the domain of different bond hybridization. In a Raman spectrum, chemisorption of FEBID carbon (or intermediate hydrocarbon radicals) on graphene results in the appearance of a D peak due to the generation of sp^3-type defects in graphene, even in an absence of graphitic domains in the deposit itself.[35,38] On the contrary, in the case of physisorption, defect-free graphene does not have any contribution to the D peak, and as-deposited FEBID carbon with small content of graphitic domains will have no apparent D peak in the Raman spectrum.[26,35] Accordingly, the D peak in the Raman spectrum enables identification of the nature of adsorption states (i.e., chemisorption vs physisorption) of FEBID carbon on graphene.

FEBID Carbon Patterning and Laser-Assisted Postdeposition Thermal Ablation. In the experiment, six square-shaped carbon patterns were fabricated using FEBID on a CVD monolayer graphene film supported by 90 nm SiO_2/Si substrate. We utilized an intrinsically present environmental hydrocarbon contamination adsorbed on graphene as a precursor source for FEBID process (FEI Quanta 200 ESEM at $P_{chamber} \sim 10^{-6}$ Torr with electron beam energy of 25 keV and dose of 10^{18} to 10^{19} e^-/cm^2; see the Supporting Information). In Figure 2, two distinct regions of carbon deposits can be identified after the electron beam exposure: (i) an intended FEBID carbon pattern of squares on graphene where the primary, high-energy beam electrons (25 keV) impinged on the graphene surface, and (ii) unintentional parasitic "halo" carbon film around each square formed by low-energy, secondary electrons (<50 eV).[1,2] It should be emphasized that the difference between these two types of carbon deposits is whether or not the high-energy beam electrons were the first step in the deposition sequence, which as suggested by the DFT calculations generates defects on graphene and drives chemisorption of FEBID intermediate species.

Laser-induced thermal ablation is known to effectively remove FEBID carbon and thus improve deposited material purity and pattern resolution.[39] In

particular, in our prior work, a Raman laser was found to effectively locally ablate FEBID carbon deposits on various substrates.[27] Exploiting this idea, we utilized the Raman laser (514 nm Ar^+ ion laser with 5.5 mW power) to selectively get rid of the parasitic halo carbon film. Figure 3a shows a sequence of optical images of as-deposited FEBID carbon on graphene and its removal via multiple laser exposures over the entire graphene area. Three consecutive laser thermal ablation experiments were performed, while collecting the Raman spectra at each step. Figure 3b shows the AFM topographic image of FEBID carbon on graphene after a third laser exposure. After the third laser exposure, most of the carbon halo film was removed with the reduction of the parasitic deposit thickness to vanishing levels. As shown in Figure 3c, thickness of the primary beam-irradiated square patterns also decreased by about 90% after the second laser exposure, but the third laser exposure did not lead to further noticeable changes in their thickness with an average height of residual pattern 0.8 ± 0.3 nm (rms roughness = 0.29 ± 0.04 nm). It suggests that laser-induced thermal ablation can be an effective technique to remove the parasitic carbon deposits everywhere, and only a few atomic carbon layers of a desired pattern that has been exposed to high-energy electron beam irradiation remain strongly bound to graphene.

FEBID Carbon Adsorption States and Deposit Composition on Graphene. Figure 4a,b shows the Raman maps of the integrated intensity of the G peak over the spectral range from 1500 to 1650 cm^{-1} and the D peak from 1350 to 1450 cm^{-1}, respectively. The results indicate a much greater contrast between G and D peaks for the electron-beam-irradiated square patterns than for the unintentional film deposits. Composition of as-deposited FEBID carbon is generally similar regardless of electron beam conditions, such as beam current and energy,[26] and even for different hydrocarbon precursors.[40] The number of sp^2 bonds in the as-deposited FEBID carbon, which influence the G peak in the Raman spectrum, vary proportionally to the volume of deposits. Since the area of the laser spot is identical during all Raman measurements, the effect of the deposit volume on the Raman signal depends on the deposit thickness (see Supporting Information).
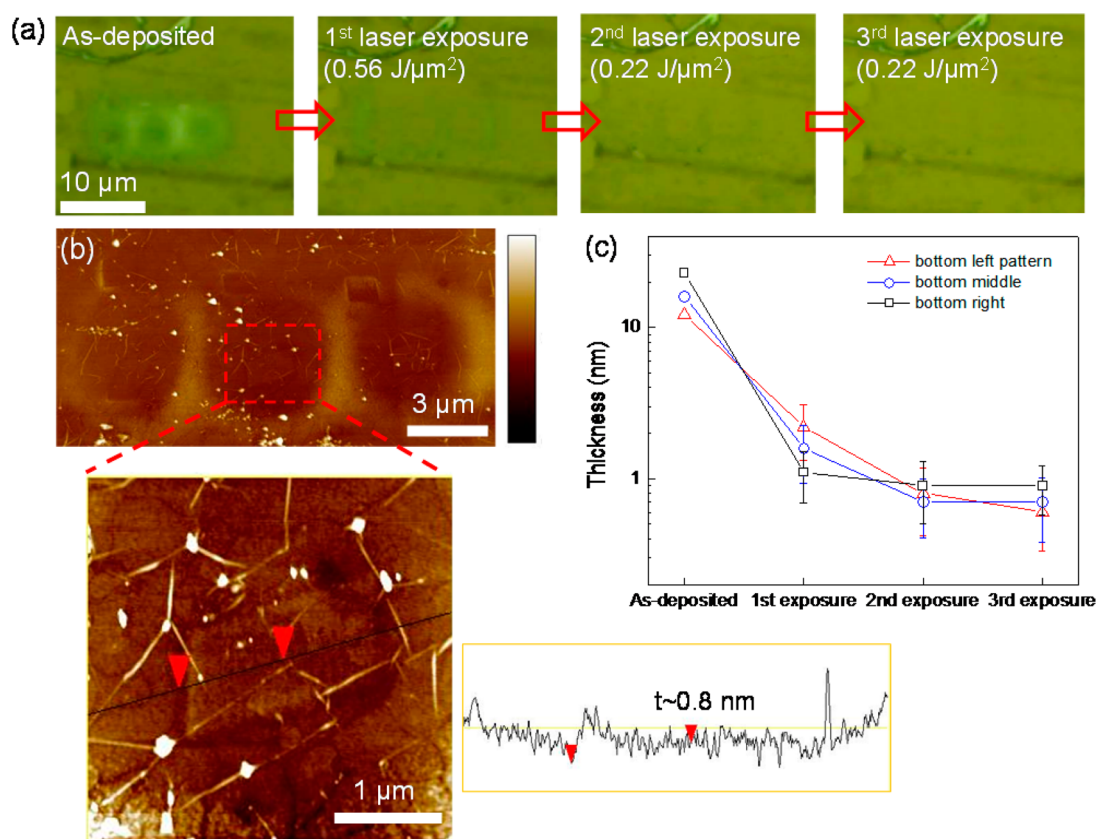
Figure 3. Visualization of FEBID-produced carbon deposits on CVD graphene: (a) optical images qualitatively showing removal of the physisorbed carbon film by high-power (5.5 mW) laser ablation; (b) AFM image of the FEBID carbon structures after third laser exposure (z-scale = 50 nm). The insets show the AFM image of the patterned carbon square (z-scale = 8 nm) and the cross-sectional profile of the patterned carbon square thickness (c) Change in the thickness of the bottom three patterned carbon squares upon the consecutive laser exposures.
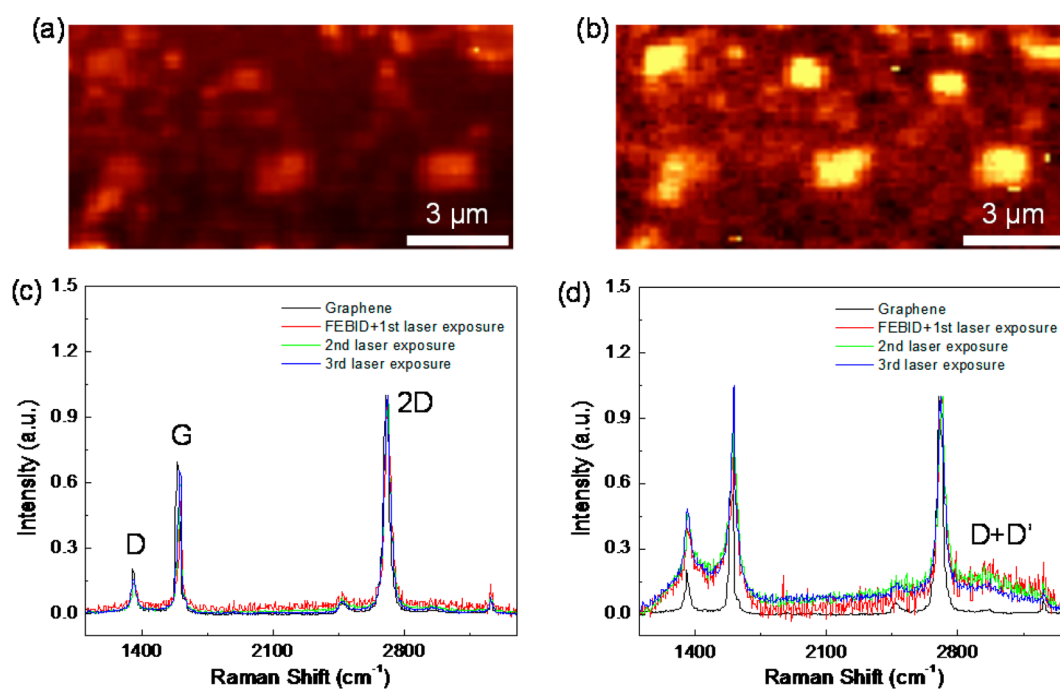

Figure 4. Raman maps showing the integrated intensity of (a) G peak and (b) D peak, and the Raman spectra for graphene areas covered with (c) physisorbed "parasitic" FEBID carbon and (d) chemisorbed FEBID patterned carbon squares, upon consecutive laser exposures.

As shown in Figures 2 and 3, the thickness of the square patterns is similar or smaller than the unintentional film deposits, and thus, the higher content of sp^2 sites (higher contrast of G peak map in Figure 4a) in the patterned domains indicates the difference in FEBID carbon composition of the high-energy beam-irradiated areas, as compared to the halo film exposed to low-energy electrons only. This suggests that carbon chemisorption occurs in the primary electron-irradiated graphene sites *versus* its physisorption in surrounding halo sites exposed only to the low-energy secondary electrons. As revealed by the DFT calculations, this is an outcome of two distinctly different mechanisms of surface interactions between the FEBID intermediate radicals and graphene depending on whether it is pristine or has structural bond defects, induced by high-energy electrons. In Figure 4b, the higher contrast of the D peak is indicative of more disordered carbon structure in the square pattern deposits. It can either result from generation of sp^3-type defects on graphene underneath directly irradiated square deposits or may also appear due to the presence of graphitic domains in the deposited carbon.[26,35,37]

Figure 4c,d represents the evolution of Raman spectra of graphene beneath the parasitic carbon halo film and patterned carbon areas, respectively, upon laser-induced thermal ablation. The Raman spectra for each patterned carbon areas are presented in the Supporting Information, providing the detailed analysis of the effect of electron beam dose on FEBID carbon formation on graphene. One can unambiguously identify the dissimilar adsorption states between the two regions. The spectrum of graphene covered by the halo carbon film in Figure 4c is similar to that of graphene itself with a small D peak and strong and narrow G and 2D peaks, which indicates the carbon film deposits have weak chemical coupling to graphene as expected for the physisorption state. In contrast, the spectrum of graphene areas covered with the high-energy electron-irradiated patterns, shown in Figure 4d, features broad G and D peaks, indicating that the FEBID carbon deposits strongly influence the spectrum even though the thickness of the square patterns (*i.e.*, the amount of deposited carbon) is less than that of the halo film. This supports the conclusion from DFT calculations that, in the case of halo carbon film, which was deposited on electron-beam-unperturbed graphene and whose adsorption state is physisorption, the carbon deposit is weakly coupled to the substrate and does not induce any structural defects in graphene. Thus, no increase/activation of the D peak is expected in the carbon film-covered graphene Raman spectrum. Also, since graphene with sp^2 hexagonal lattice structure has higher Raman scattering cross section,[35,41] the deposits with low content of sp^2 sites, due to the lack of graphitic domains,[26,27] give small contributions to the G peak of the Raman spectrum

even when a deposited carbon film is at least 50 times thicker than the graphene support itself.

In the case of the square carbon patterns whose adsorption state is chemisorption, the carbon deposits undergo local rehybridization of sp^2- to sp^3-like bonds of graphene upon exposure to high-energy primary electrons, as shown by the DFT calculations. Accordingly, this increases the number of defects and, at the same time, also reduces the content of sp^2 hexagonal sites on graphene. Despite the reduction of intrinsic sp^2 hexagonal sites on graphene, the carbon deposition onto the defect sites contributes additional sp^2 carbon bonds in the form of chains or rings, which cumulatively increases the intensity and broadens the G peak. Additionally, a pronounced, broad D peak and appearance of D + D' peak (at $\sim$2940 cm^{-1}) shown in the spectrum are the Raman signatures of amorphous carbon with imbedded nanocrystalline size of graphitic domains.[26,37] Therefore, we can conclude that chemisorption of intermediate hydrocarbon radicals and ultimately of the carbon deposit on high-energy electron-beam-impacted areas of graphene facilitates intimate coupling between the graphene substrate and FEBID carbon with an increased formation of sp^2 sites of graphitic domains (see Supporting Information on control experiments using a bare SiO_2/Si substrate).

To quantify the difference between the two types of carbon deposits onto graphene, the D to G peak intensity and area ratios, denoted as $I(D)/I(G)$ and $A(D)/A(G)$, are plotted in Figure 5a,b, respectively. The intensity ratio is generally used as a measure of point-like defects on graphene,[37,38] while the area ratio can be used to determine the composition of amorphous carbon.[26,27,35] In Figure 5a, the intensity ratio changes little in the graphene areas covered with the carbon halo film, but it profoundly increases in the graphene areas with the carbon square deposits which were irradiated by high-energy primary electrons. This further supports the conclusion about differences in the adsorption state of carbon deposited onto graphene areas which have (*i.e.*, chemisorption sites with strong carbon–graphene interactions) and have not (*i.e.*, physisorption sites with weak carbon–graphene interactions) been exposed to direct irradiation of high-energy electron beam, owing to formation of structural defects in graphene substrate during the FEBID process. Interestingly, subsequent annealing *via* laser exposure essentially fully removes carbon from the physisorbed film areas but does not make a significant change in the Raman peak intensity ratio for both physisorbed and chemisorbed carbon deposit states.

In Figure 5b, the D to G peak area ratio, $A(D)/A(G)$, increases to $\sim$1.4 after deposition and first annealing step *via* laser exposure for both the physisorbed carbon film and chemisorbed carbon squares. However, after additional laser exposures (second and third),
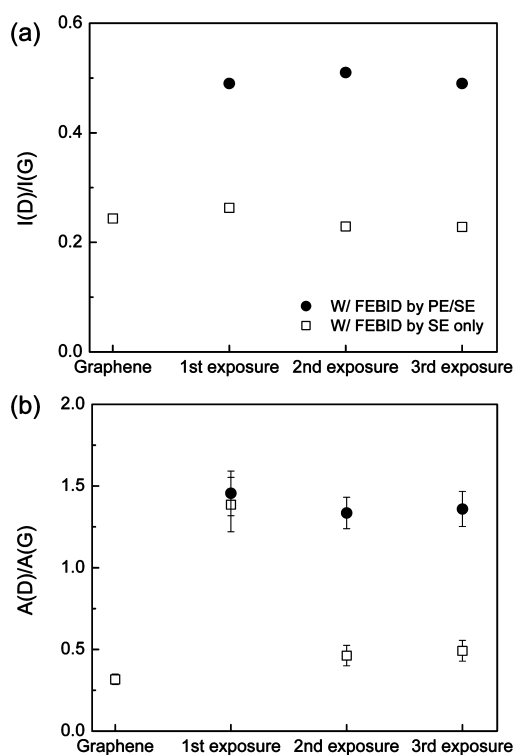
Figure 5. Change of (a) intensity and (b) area ratios of the D to the G peaks for graphene areas with FEBID carbon deposits exposed to both high-energy primary electrons and low-energy secondary electrons (FEBID by PE/SE, shown using filled symbols) and those exposed to secondary electrons only (FEBID by SE only), showing the progression through multiple laser exposures for thermal ablation.

A(D)/A(G) for the physisorbed carbon film is noticeably decreased close to that of pristine graphene due to ablation of weakly bound carbon film, which is the source of perturbations for the graphene Raman spectrum. It indicates that laser-induced thermal ablation of physisorbed halo carbon deposits does not damage graphene and could be potentially used as a safe means for cleaning the graphene layer from carbon "contaminants" of the electron beam patterning process. In contrast, for the chemisorbed carbon, there is no significant change of the A(D)/A(G) ratio around 1.3−1.5 upon consecutive laser exposures, which

indicates that the laser annealing does not alter the compositions of the chemisorbed carbon structure. It suggests that only a few layers of as-deposited carbon atoms remain on the surface covalently bound to graphene and contribute to the Raman spectrum. The area ratio indicates that the chemisorbed carbon is amorphous with graphitic cluster size of ∼1.7 nm,[35] confirming that chemisorption of electron-stimulated dissociation precursor radicals onto graphene leads to graphitization of FEBID carbon deposits.

CONCLUSION

In summary, we discovered two possible adsorption states of carbon deposits on graphene, which are fabricated by FEBID. Using DFT calculations, it was shown that the sp^3-type defects in graphene produced by high-energy beam electrons form energetically favorable sites for chemisorption of FEBID-produced intermediate hydrocarbon species onto graphene. The different adsorption states during the FEBID process were confirmed using Raman spectroscopy of FEBID carbon deposits in combination with postdeposition multistep laser annealing/ablation. It was shown that weakly coupled physisorbed FEBID carbon formed in the surrounding areas of graphene substrate with no direct exposure to high-energy electrons can be effectively eliminated by laser-induced thermal ablation with no damage to graphene. In contrast, the chemisorbed FEBID carbon on the areas with graphene structural defects induced by electron beam irradiation "survives" laser ablation treatment in the form of a few atomic layers of carbon atoms covalently bonded to graphene. This study provides a fundamental insight into the interactions between FEBID-produced carbon deposits and graphene, which is foundational for electron-beam-based direct-write graphene nanopatterning. In combination with demonstrated postdeposition "cleaning" process using laser ablation to remove detrimental halo carbon deposits with graphene remaining intact, it establishes the FEBID as a novel tool for controlled covalent functionalization of graphene with applications to electronic device fabrication.

METHODS

Theory. To evaluate possible CH_3 radical adsorption states, we performed geometry optimization using the generalized gradient approximation Perdew−Burke−Ernzerhof (PBE) functional[20,21,42] for the exchange correlation potential of interaction electrons with double numerical basis set in DMol3.[43] Self-consistent field convergence, 10^{-5} Ha, was obtained at the $9 \times 9 \times 1$ Monkhorst−Pack (MP) k-point grid. To assess only the effect of the defect height on adsorption, we fixed the coordinates of all carbon atoms in defected graphene, while a CH_3 radical was not constrained.

Experiment. CVD graphene grown on Cu foil was transferred to a 90 nm SiO_2/Si substrate using a PMMA-mediated wet transfer method[44] with an aqueous solution of ammonium persulfate (0.05 g/mL) as a Cu etchant. Monolayer graphene

was confirmed with a sharp, intense 2D peak shape in the Raman spectrum (Figure 4).[45] Topography images (Figures 2a and 3b) were obtained using a Dimension-3000 microscope with a silicon tip in a tapping mode. Laser-induced thermal ablation and Raman measurements of FEBID carbon on graphene were carried out with a WITec (Alpha 300R) confocal Raman microscope using 514.5 nm Ar$^+$ ion laser with a maximum power of ∼5.5 mW, and 10^4 laser spots with 1 μm spot size exposed scanning areas over graphene for a total of ∼3 h (1.1 s dwelling time per one laser spot). The scanning areas were set as 10 μm × 10 μm for first laser exposure and 16 μm × 16 μm for second and third laser exposures, yielding different thermal energy per unit area transferred to the graphene sample, as indicated in Figure 3a. The Raman data were analyzed for the spectral range between 1100 and 1750 cm^{-1} to see the G and D

peaks. Lorentzian peak fitting was applied to the Raman data in order to obtain the D to G peak intensity and area ratios.

Conflict of Interest: The authors declare no competing financial interest.

Supporting Information Available: The electron beam conditions set for FEBID carbon patterning on graphene, the effect of primary electron beam dose on chemisorption of FEBID carbon on graphene, and control experiments for FEBID carbon deposition on a bare SiO_2/Si substrate. This material is available free of charge *via* the Internet at http://pubs.acs.org.

REFERENCES AND NOTES

1. Randolph, S. J.; Fowlkes, J. D.; Rack, P. D. Focused, Nanoscale Electron-Beam-Induced Deposition and Etching. *Crit. Rev. Solid State Mater. Sci.* **2006**, *31*, 55–89.
2. van Dorp, W. F.; Hagen, C. W. A Critical Literature Review of Focused Electron Beam Induced Deposition. *J. Appl. Phys.* **2008**, *104*, 081301.
3. Rykaczewski, K.; White, W. B.; Fedorov, A. G. Analysis of Electron Beam Induced Deposition (EBID) of Residual Hydrocarbons in Electron Microscopy. *J. Appl. Phys.* **2007**, *101*, 054307.
4. van Dorp, W. F.; van Someren, B.; Hagen, C. W.; Kruit, P. Approaching the Resolution Limit of Nanometer-Scale Electron Beam-Induced Deposition. *Nano Lett.* **2005**, *5*, 1303–1307.
5. Banhart, F. The Formation of a Connection between Carbon Nanotubes in an Electron Beam. *Nano Lett.* **2001**, *1*, 329–332.
6. Rykaczewski, K.; Henry, M. R.; Kim, S. K.; Kulkarni, D.; Singamaneni, S.; Tsukruk, V. V.; Fedorov, A. G. Effect of Electron Beam Induced Deposited (EBID) Carbon Joint Geometry and Material Properties on Electrical Resistance of Multiwalled Carbon Nanotubes (MWNT)-to-Metal Contact Interface. *Nanotechnology* **2010**, *21*, 0352021.
7. Kim, S.; Kulkarni, D. D.; Rykaczewski, K.; Henry, M.; Tsukruk, V. V.; Fedorov, A. G. Fabrication of an Ultralow-Resistance Ohmic Contact to MWCNT-Metal Interconnect Using Graphitic Carbon by Electron Beam Induced Deposition (EBID). *IEEE Trans. Nanotechnol.* **2012**, *11*, 1223–1230.
8. Hoeflich, K.; Yang, R. B.; Berger, A.; Leuchs, G.; Christiansen, S. The Direct Writing of Plasmonic Gold Nanostructures by Electron-Beam-Induced Deposition. *Adv. Mater.* **2011**, *23*, 2657–2661.
9. Kurra, N.; Bhadram, V. S.; Narayana, C.; Kulkarni, G. U. Field-Effect Transistors Based on Thermally Treated Electron Beam-Induced Carbonaceous Patterns. *ACS Appl. Mater. Interfaces* **2012**, *4*, 1030–1036.
10. Boero, G.; Utke, I.; Bret, T.; Quack, N.; Todorova, M.; Mouaziz, S.; Kejik, P.; Brugger, J.; Popovic, R. S.; Hoffmann, P. Submicrometer Hall Devices Fabricated by Focused Electron-Beam-Induced Deposition. *Appl. Phys. Lett.* **2005**, *86*, 042503.
11. Bernau, L.; Gabureac, M.; Erni, R.; Utke, I. Tunable Nanosynthesis of Composite Materials by Electron-Impact Reaction. *Angew. Chem., Int. Ed.* **2010**, *49*, 8880–8884.
12. Bishop, J.; Lobo, C. J.; Martin, A.; Ford, M.; Phillips, M.; Toth, M. Role of Activated Chemisorption in Gas-Mediated Electron Beam Induced Deposition. *Phys. Rev. Lett.* **2012**, *109*, 146103.
13. Muthukumar, K.; Opahle, I.; Shen, J.; Jeschke, H. O.; Valenti, R. Interaction of $W(CO)_6$ with SiO_2 Surfaces: A Density Functional Study. *Phys. Rev. B* **2011**, *84*, 205442.
14. Banhart, F.; Kotakoski, J.; Krasheninnikov, A. V. Structural Defects in Graphene. *ACS Nano* **2010**, *5*, 26–41.
15. Meyer, J. C.; Eder, F.; Kurasch, S.; Skakalova, V.; Kotakoski, J.; Park, H. J.; Roth, S.; Chuvilin, A.; Eyhusen, S.; Benner, G.; *et al.* Accurate Measurements of Electron Beam Induced Displacement Cross Sections for Single-Layer Graphene. *Phys. Rev. Lett.* **2012**, *108*, 196102.
16. Jones, J. D.; Mahajan, K. K.; Williams, W. H.; Ecton, P. A.; Mo, Y.; Perez, J. M. Formation of Graphene and Partially Hydrogenated Graphene by Electron Irradiation of Adsorbates on Graphene. *Carbon* **2010**, *48*, 2335–2340.
17. Ryu, S.; Han, M. Y.; Maultzsch, J.; Heinz, T. F.; Kim, P.; Steigerwald, M. L.; Brus, L. E. Reversible Basal Plane Hydrogenation of Graphene. *Nano Lett.* **2008**, *8*, 4597–4602.
18. Balakrishnan, J.; Koon, G. K. W.; Jaiswal, M.; Neto, A. H. C.; Oezyilmaz, B. Colossal Enhancement of Spin−Orbit Coupling in Weakly Hydrogenated Graphene. *Nat. Phys. Lett.* **2013**, *9*, 284–287.
19. Elias, D. C.; Nair, R. R.; Mohiuddin, T. M. G.; Morozov, S. V.; Blake, P.; Halsall, M. P.; Ferrari, A. C.; Boukhvalov, D. W.; Katsnelson, M. I.; Geim, A. K.; *et al.* Control of Graphene's Properties by Reversible Hydrogenation: Evidence for Graphane. *Science* **2009**, *323*, 610–613.
20. Santos, E. J. G.; Ayuela, A.; Sanchez-Portal, D. Universal Magnetic Properties of sp^3-Type Defects in Covalently Functionalized Graphene. *New J. Phys.* **2012**, *14*, 043022.
21. Boukhvalov, D. W.; Katsnelson, M. I. A New Route towards Uniformly Functionalized Single-Layer Graphene. *J. Phys. D: Appl. Phys.* **2010**, *43*, 175302.
22. Zhou, Y. G.; Wang, Z. G.; Yang, P.; Zu, X. T.; Xiao, H. Y.; Sun, X.; Khaleel, M. A.; Gao, F. Electronic and Magnetic Properties of C-Adsorbed Graphene: A First-Principles Study. *Phys. Chem. Chem. Phys.* **2011**, *13*, 16574–16578.
23. Ataca, C.; Aktürk, E.; Sahin, H.; Ciraci, S. Adsorption of Carbon Adatoms to Graphene and Its Nanoribbons. *J. Appl. Phys.* **2011**, *109*, 013704.
24. Gerber, I. C.; Krasheninnikov, A. V.; Foster, A. S.; Nieminen, R. M. A First-Principles Study on Magnetic Coupling between Carbon Adatoms on Graphene. *New J. Phys.* **2010**, *12*, 113021.
25. Jin, C. H.; Wang, J. Y.; Chen, Q.; Peng, L. M. *In Situ* Fabrication and Graphitization of Amorphous Carbon Nanowires and Their Electrical Properties. *J. Phys. Chem. B* **2006**, *110*, 5423–5428.
26. Kulkarni, D. D.; Rykaczewski, K.; Singamaneni, S.; Kim, S.; Fedorov, A. G.; Tsukruk, V. V. Thermally Induced Transformation of Amorphous Carbon Nanostructures Fabricated by Electron Beam Induced Deposition. *ACS Appl. Mater. Interfaces* **2011**, *3*, 710–720.
27. Kulkarni, D. D.; Kim, S.; Fedorov, A. G.; Tsukruk, V. V. Light-Induced Plasmon-Assisted Phase Transformation of Carbon on Metal Nanoparticles. *Adv. Funct. Mater.* **2012**, *22*, 2129–2139.
28. van Dorp, W. F.; Zhang, X.; Feringa, B. L.; Hansen, T. W.; Wagner, J. B.; De Hosson, J. Th. M. Molecule-by-Molecule Writing Using a Focused Electron Beam. *ACS Nano* **2012**, *6*, 10076–10081.
29. Meyer, J. C.; Girit, C. O.; Crommie, M. F.; Zettl, A. Hydrocarbon Lithography on Graphene Membranes. *Appl. Phys. Lett.* **2008**, *92*, 123110.
30. Thierfelder, C.; Witte, M.; Blankenburg, S.; Rauls, E.; Schmidt, W. G. Methane Adsorption on Graphene from First Principles Including Dispersion Interaction. *Surf. Sci.* **2011**, *605*, 746–749.
31. Mandeltort, L.; Choudhury, P.; Johnson, J. K.; Yates, J. T. Reaction of the Basal Plane of Graphite with the Methyl Radical. *J. Phys. Chem. Lett.* **2012**, *3*, 1680–1683.
32. Koh, W.; Choi, J. I.; Lee, S. G.; Lee, W. R.; Jang, S. S. First-Principles Study of Li Adsorption in a Carbon Nanotube−Fullerene Hybrid System. *Carbon* **2011**, *49*, 286–293.
33. Li, L.; Reich, S.; Robertson, J. Defect Energies of Graphite: Density-Functional Calculations. *Phys. Rev. B* **2005**, *72*, 184109.
34. Banhart, F. Irradiation Effects in Carbon Nanostructures. *Rep. Prog. Phys.* **1999**, *62*, 1181–1221.
35. Ferrari, A. C.; Robertson, J. Interpretation of Raman Spectra of Disordered and Amorphous Carbon. *Phys. Rev. B* **2000**, *61*, 14095.

36. Dresselhaus, M. S.; Jorio, A.; Hofmann, M.; Dresselhaus, G.; Saito, R. Perspectives on Carbon Nanotubes and Graphene Raman Spectroscopy. *Nano Lett.* **2010**, *10*, 751–758.

37. Cancado, L. G.; Jorio, A.; Martins Ferreira, E. H.; Stavale, F.; Achete, C. A.; Capaz, R. B.; Moutinho, M. V. O.; Lombardo, A.; Kulmala, T. S.; Ferrari, A. C. Quantifying Defects in Graphene *via* Raman Spectroscopy at Different Excitation Energies. *Nano Lett.* **2011**, *11*, 3190–3196.

38. Eckmann, A.; Felten, A.; Mishchenko, A.; Britnell, L.; Krupke, R.; Novoselov, K. S.; Casiraghi, C. Probing the Nature of Defects in Graphene by Raman Spectroscopy. *Nano Lett.* **2012**, *12*, 3925–3930.

39. Roberts, N. A.; Fowlkes, J. D.; Magel, G. A.; Rack, P. D. Enhanced Material Purity and Resolution *via* Synchronized Laser Assisted Electron Beam Induced Deposition of Platinum. *Nanoscale* **2013**, *5*, 408–415.

40. Bret, T.; Mauron, S.; Utke, I.; Hoffmann, P. Characterization of Focused Electron Beam Induced Carbon Deposits from Organic Precursors. *Microelectron. Eng.* **2005**, *78−79*, 300–306.

41. Kudin, K. N.; Ozbas, B.; Schniepp, H. C.; Prud'homme, R. K.; Aksay, I. A.; Car, R. Raman Spectra of Graphite Oxide and Functionalized Graphene Sheets. *Nano Lett.* **2008**, *8*, 36–41.

42. Perdew, J. P.; Burke, K.; Ernzerhof, M. Generalized Gradient Approximation Made Simple. *Phys. Rev. Lett.* **1996**, *77*, 3865–3868.

43. Delley, B. From Molecules to Solids with the DMol3 Approach. *J. Chem. Phys.* **2000**, *113*, 7756–7764.

44. Li, X.; Zhu, Y.; Cai, W.; Borysiak, M.; Han, B.; Chen, D.; Piner, R. D.; Colombo, L.; Ruoff, R. S. Transfer of Large-Area Graphene Films for High-Performance Transparent Conductive Electrodes. *Nano Lett.* **2009**, *9*, 4359–4363.

45. Martins Ferreira, E. H.; Moutinho, M. V. O.; Stavale, F.; Lucchese, M. M.; Capaz, R. B.; Achete, C. A.; Jorio, A. Evolution of the Raman Spectra from Single-, Few-, and Many-Layer Graphene with Increasing Disorder. *Phys. Rev. B* **2010**, *82*, 125429.